Springer

KSME

Journal of Mechanical Science and Technology 28 (10) (2014) 4109~4119
www.springerlink.com/content/1738-494x
DOI 10.1007/s12206-014-0950-4

Periodic transonic flow simulation using fourier-based algorithm †

Mohammad Reza Mohaghegh[1,*] and Majid Malek-Jafarian[2]

[1]*Young Researchers and Elite Club, Torbat-e Heydarieh Branch, Islamic Azad University, Torbat-e Heydarieh, Iran*
[2]*Department of Mechanical Engineering, University of Birjand, Birjand, Iran*

(Manuscript Received January 8, 2014; Revised June 30, 2014; Accepted July 18, 2014)

Abstract

The present research simulates time-periodic unsteady transonic flow around pitching airfoils via the solution of unsteady Euler and Navier-Stokes equations, using time spectral method (TSM) and compares it with the traditional methods like BDF and explicit structured adaptive grid method. The TSM uses a Fourier representation in time and hence solves for the periodic state directly without resolving transients (which consume most of the resources in a time-accurate scheme). Mathematical tools used here are discrete Fourier transformations. The TSM has been validated with 2D external aerodynamics test cases. These test cases are NACA 64A010 (CT6) and NACA 0012 (CT1 and CT5) pitching airfoils. Because of turbulent nature of flow, Baldwin-Lomax turbulence model has been used in viscous flow analysis with large oscillation amplitude (CT5 type). The results presented by the TSM are compared with experimental data and the two other methods. By enforcing periodicity and using Fourier representation in time that has a spectral accuracy, tremendous reduction of computational cost has been obtained compared to the conventional time-accurate methods. Results verify the small number of time intervals per pitching cycle (just four time intervals) required to capture the flow physics with small oscillation amplitude (CT6) and large oscillation amplitude (CT5) as compared to the other two methods.

Keywords: Time spectral method (TSM); Time-periodic unsteady flow; Discrete Fourier transform; Pitching airfoil; Baldwin-Lomax turbulence model

1. Introduction

Unsteady flow calculations have been used extensively, including in flutter analysis, analysis of flow around helicopter blades etc. In these matters, flow behavior is often unsteady but periodic.

The investigation and solution of periodic unsteady flows past oscillating airfoils is useful and widely used in aeronautical applications. One of the pioneering and comprehensive studies in this field is by McCroskey [1, 2], who performed comprehensive study on the behavior of unsteady airfoil. Further researches involving various numerical methods to simulate periodic unsteady flow have been performed such as by Rausch et al. [3], Anderson et al. [4], Mittal [5], Yang et al. [6], Zhao et al. [7], and Yang et al. [8].

In analyzing these problems, algorithms that can use the periodic property of flow can be useful. Traditional time stepping methods do not consider this property. Explicit schemes for stability use small time steps but this is time-consuming. Implicit schemes, use a larger range of time steps, but because of the long repeat process to achieve solution convergence, these schemes are expensive, especially for three-dimensional problems. Time accurate solvers like the implicit second-order backward difference formula (BDF) require integration on several periods with small time steps to achieve periodic steady state. It takes a long time. Many searches have been done in this area, inclusive of recent works of Hsu and Jameson [9] and Nadarajah and Jameson [10], Hsu [11], Zhang et al. [12].

The significant issue concerning numerical solution is the balance between computation time and solution accuracy. In traditional schemes, because of limited use of small time steps (and consequently, a multitude of number of time steps) some procedures such as explicit structured adaptive grid method (Pasandideh Fard et al., [13]) are inherently time-consuming. Moreover, on other schemes like BDF, if broad time steps are chosen, the accuracy of solution wanes, and when time steps are small-scale, solving time tends to increase. Therefore, a suitable algorithm is the one that, apart from reducing solving time, keeps up the proper accuracy.

In recent years, researchers have turned to using Fourier-based algorithms to significantly reduce the computational expense for analyzing unsteady periodic problems. Hall et al. [14] did the first study in this field. They proposed the harmonic balanced method for solving nonlinear equations in frequency space. Also, one can refer to some other researches using harmonic balance technique such as Thomas

*Corresponding author. Tel.: +98 5312294958, Fax.: +98 5312094952
E-mail address: mr.mohaghegh@me.iut.ac.ir
† Recommended by Associate Editor Kyu Hong Kim
© KSME & Springer 2014

[15-17], Spiker at al. [18], Liu et al. [19, 20], and Ronch et al. [21].

Subsequently, McMullen et al., [22-24] introduced the non-linear frequency domain (NLFD) method. In this method, equations are first converted to frequency space and then solved in frequency space, while the flow variables are returned into the physical space. So, to use this method, substantial changes in existent flow solvers are required, since the method needs to use fast Fourier transform (FFT) and inverse fast Fourier transform (IFFT). Nadarajah et al. [25, 26] used NLFD method for optimum shape design of unsteady three-dimensional viscous flows. Subsequently, Cagnone and Nadarajah [27] investigated an implicit non-linear frequency domain-spectral difference scheme for periodic Euler flow. And recently Mosahebi and et al. [28] studied dynamic mesh deformation for implicit adaptive NLFD method.

Since the use of NLFD method requires the application of FFT and IFFT, great changes must be utilized for a time accurate unsteady flow solver. Gopinath and Jameson [29] proposed using a Fourier collocation matrix for the temporal derivative term and time integration to prevent FFT, IFFT and the use of minimal changes in the time accurate flow solver. This scheme is called time spectral method (TSM). Subsequently, Butsuntorn and Jameson [30, 31] used TSM for rotorcraft flow. Then Sicot et al. [32] presented the Block-Jacobi approach to solve stationary problems with an implicit algorithm for TSM. Su, and Yuan [33] applied implicit solution of time spectral method for periodic unsteady flows. Yang and Mavriplis [34, 35] used TSM for periodic and quasi-periodic unsteady computations on unstructured meshes. Antheaume and Corre [36] simulated periodic incompressible flows using implicit TSM.

In TSM, the time derivative term couples all the time levels of solution in each period through Fourier collocation matrix. Unlike finite difference methods that use only several solution variables related to preceding (explicit) times or succeeding (implicit) ones to calculate the derivative term in an individual time level, TSM uses all the time levels in a period (as a high-order method) in calculating the derivative term, and therefore it shows very high accuracy. Unlike time marching methods, the flow variables have been solved simultaneously at all instances and this process repeats until it reaches a periodic steady state. The detailed algorithm of this technique will be presented in next section.

Because of the flow turbulence nature of the physical problem in this research, a turbulence model should be applied at viscous flow analysis. This paper tries using reliable models while being very simple to implement. Turbulence modelling is applied with an algebraic model by Baldwin and Lomax [37] which has the advantage of being simple to implement compared to the kε and kω models.

Most of the earliest turbulence models were based on Prandtl's mixing length theory. Prandtl [38] suggested a mixing length that relates the eddy viscosity to the local mean velocity gradient. The reason for successful applications of the mixing length theory is to find some general method using the definition of the mixing length. Most algebraic models divide the boundary layer into two regions, an inner and an outer region. The inner layer is composed of the viscous sublayer, the buffer layer, and part of the fully turbulent log region. The outer layer includes the remaining part of the log layer and the wake region.

Cebeci-Smith [39] suggested a model that is fairly simple, but it requires knowledge of the conditions at the edge of the boundary layer and the boundary layer thickness. These quantities are not always easy to calculate in complicated flows with a Navier-Stokes code since it is often difficult to define where the boundary layer edge actually occurs

Baldwin-Lomax extended a model of the outer eddy viscosity that did not require knowledge of the conditions at the edge of the boundary layer. This model has become quite popular for CFD applications.

We used TSM with Baldwin-Lomax turbulence model for simulation of 2D external aerodynamics test cases as pitching airfoils. These test cases are NACA 64A010 test case 6 (CT6) with small oscillation amplitude, weak shock waves and reduced frequency higher than NACA 0012 test cases and NACA 0012 test cases 1 and 5 (CT1 and CT5) with large oscillation amplitude, strong shock waves and reduced frequency lower proportion. The numerical results are compared with experimental data. Two different airfoils, the NACA 64A010 and the NACA 0012, were tested by Davis [40] and Landon [41], respectively. The experimental data was published as part of AGARD report 702. A factor contributing to its selection was its popularity in the numerical-analysis community. These airfoils are famous for testing of numerical methods and so those are used in researches of others repeatedly.

Due to the 64A010 airfoil properties (according to Table 1) this airfoil is for a transonic symmetric airfoil oscillating over a limited range in angle of attack. Because of this fairly small variation in angle of attack, the numerical results are considered to be less sensitive to the choice of turbulence model than the data for the 0012 airfoil that has fairly big variation in angle of attack. So, Navier-Stokes simulation with turbulent model is used for 0012 airfoil (CT5).

In the following sections, we first verify the accuracy of the spatial discretization of the TSM by running it for CT1 in an inviscid flow and compare its results to experimental data. These comparisons confirm the size of grids used for the unsteady cases. Then we used CT6 for Euler equations simulation and CT5 for Navier- Stokes equations simulation with Baldwin-Lomax turbulence model.

Finally, numerical results of TSM have been compared with the BDF and explicit structured adaptive grid methods for surveying efficiency TSM in time periodic problems simulation. To our knowledge, such extensive comparative analysis was not available when work on this paper started. In this research, the efficiency of TSM has been shown by these comparisons.

2. Governing equations

Because of the flow turbulent nature of the physical problem studied in this research, a turbulence model should be applied to viscous flow analysis.

2.1 Conservative form of the field equations

The two-dimensional conservative form of the Navier-Stokes equation in Cartesian coordinates is:

$$\frac{\partial w}{\partial t}+\frac{\partial f}{\partial x}+\frac{\partial g}{\partial y}=\frac{\partial f_v}{\partial x}+\frac{\partial g_v}{\partial y}, \tag{1}$$

where the state vector w, inviscid flux vectors f and g and viscous flux vector f_v and g_v are described respectively by

$$w=\begin{bmatrix}\rho\\ \rho u\\ \rho v\\ \rho e\end{bmatrix}, \tag{2}$$

$$f=\begin{bmatrix}\rho(u-x_t)\\ \rho u(u-x_t)+p\\ \rho v(u-x_t)\\ \rho e(u-x_t)+pu\end{bmatrix}, g=\begin{bmatrix}\rho(v-y_t)\\ \rho u(v-y_t)\\ \rho v(v-y_t)+p\\ \rho e(v-y_t)+pv\end{bmatrix}, \tag{3}$$

$$f_v=\begin{bmatrix}0\\ \tau_{xx}\\ \tau_{xy}\\ u\tau_{xx}+v\tau_{xy}-q_x\end{bmatrix}, g_v=\begin{bmatrix}0\\ \tau_{xx}\\ \tau_{xy}\\ u\tau_{xx}+v\tau_{xy}-q_x\end{bmatrix}, \tag{4}$$

where ρ is the density, u and v are velocity components at x and y directions, respectively, x_t and y_t are velocity components of grid, p is pressure and e is the total energy per unit mass. As, temperature T and total energy e per unit mass are determined by the ideal gas equation of state:

$$e=\frac{p}{\rho(\gamma-1)}+\frac{1}{2}(u^2+v^2), \tag{5}$$

$$T=\frac{p}{\rho R}, \tag{6}$$

where R is the gas constant.

A second-order central difference scheme is used for spatial discretization of convective flux vectors with an artificial dissipation scheme. In fact, the combination of the artificial dissipation term with central difference scheme makes a scheme similar to upwind schemes, so it can capture shock waves appropriately and well. In the present work, the Jameson-Schmidt-Turkel (JST) [42] scheme is used as the artificial dissipation scheme where mixed first- and third-order dissipation terms are presented to suppress spurious modes and ensure stability.

2.2 The time spectral method

The core of this method is based on discrete Fourier transformation for solving periodic unsteady partial differential equations. The discrete Fourier transform of w, for a time period of T, is given by:

$$\hat{w}_k=\frac{1}{N}\sum_{n=0}^{N-1}w^n e^{-ik\frac{2\pi}{T}n\Delta t}, \tag{7}$$

and its inverse transform,

$$w^n=\begin{cases}\sum_{k=-\frac{N}{2}}^{\frac{N}{2}-1}\hat{w}_k e^{ik\frac{2\pi}{T}n\Delta t} & : \text{N is even}\\ \sum_{k=-\frac{N-1}{2}}^{\frac{N-1}{2}}\hat{w}_k e^{ik\frac{2\pi}{T}n\Delta t} & : \text{N is odd}\end{cases} \tag{8}$$

where the time period T is divided into N time intervals, $\Delta t=T/N$.

The Fourier transform of the derivative approximations at nth time interval is computed by [43]:

$$D_t w^n=\frac{2\pi}{T}\sum_{j=0}^{N-1}d_n^j w^j, \tag{9}$$

where d_n^j is defined by

$$d_n^{jeven}=\begin{cases}\frac{1}{2}(-1)^{n-j}\cot(\frac{\pi(n-j)}{N}) & : n\neq j\\ 0 & : n=j\end{cases} \tag{10a}$$

and

$$d_n^{jodd}=\begin{cases}\frac{1}{2}(-1)^{n-j}\operatorname{cosec}(\frac{\pi(n-j)}{N}) & : n\neq j\\ 0 & : n=j.\end{cases} \tag{10b}$$

Since here flow is periodic in time, flow variables (the state vector w) vary periodically by time, too. Therefore, its derivative can be expressed using Eq. (9). Suppose that the cell volume ∀ does not vary in time, so the semi-discrete form of the governing Eq. (1) is:

$$\forall D_t w^n+R(w^n)=0, \tag{11}$$

where $R(W)=\frac{\partial f_i}{\partial x_i}+\frac{\partial f_{iv}}{\partial x_i}$ includes the summation of inviscid

flux and viscous vectors. Introducing pseudo time, τ, to Eq. (12) in the same manner as the explicit dual time stepping scheme,

$$\forall \frac{dw^n}{d\tau} + \forall D_t w^n + R(w^n) = 0 . \quad (12)$$

The spatial discretization scheme used for this purpose is a conservative cell-centered finite volume scheme. A local time stepping is used for accelerating convergence, in which a pseudo-time step with a five-stage Runge-Kutta time stepping scheme is performed at each level. The Runge-Kutta time stepping scheme can be written as:

$$\begin{aligned} w^{(0)} &= w^{(m)} \\ w^{(1)} &= w^{(0)} - \alpha_1 \Delta t R(w^{(0)}) \\ &\cdots \\ w^{(K)} &= w^{(0)} - \alpha_k \Delta t R(w^{(k-1)}) \\ &\cdots \\ w^{(m+1)} &= w^{(M)} \end{aligned} \quad (13)$$

where m is the number of iterations in pseudo-time and M is the total number of stages. In this work, a modified five stage Runge-Kutta scheme (Jameson [44]) is used with coefficients Eq. (15) to maximize the stability:

$$\alpha_1 = \frac{1}{4},\ \alpha_2 = \frac{1}{6}\ \alpha_3 = \frac{3}{8},\ \alpha_4 = \frac{1}{4}\ \alpha_5 = 1 \ .$$

2.3 Boundary conditions

Solid surface boundary conditions

For inviscid flow, the velocity at the wall must be tangent to the slope of the wall. This corresponds to a zero flux through the wall and thus:

$$(\hat{v}.\hat{n})_{surface} = 0 ,$$

where $\hat{n}$ is the wall surface unit normal vector. For viscous flow, the no-injection and no-slip conditions are imposed and requires an additional boundary condition to the one above

$$(\hat{v}.\hat{t})_{surface} = 0 ,$$

where $\hat{t}$ is the wall unit tangent vector. This effectively means that the velocity at the wall is zero. The above boundary conditions satisfy the momentum equation. For the case of the energy equation, an adiabatic boundary condition is employed and defined as:

$$(\hat{q}.\hat{n})_{surface} = 0 .$$

This translates to a zero heat flux through the normal of the wall. The density at the airfoil surface is extrapolated from the interior using the following expression:

$$(\frac{\partial \rho}{\partial n})_{surface} = 0 .$$

Also the pressure gradient at the surface is zero. That is:

$$(\frac{\partial P}{\partial n})_{surface} = 0 .$$

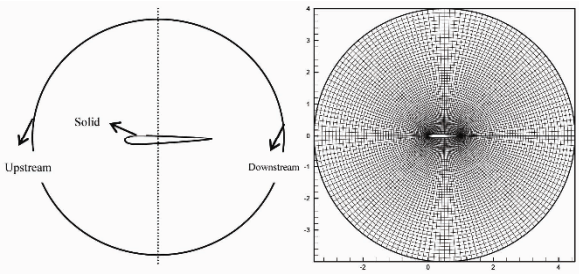

Fig. 1. The inner and outer boundary conditions for O- Grid mesh.

Far-field conditions

The outer boundary is usually placed far from the airfoil surface, at least three to five chords away. In this work, boundary conditions are used at the inner and outer boundary as shown in Fig. 1.

According to the transonic flow in this study, flow quantities (ρ,u, v, and P) in inflow boundary (upstream) are fixed to the free-stream values:

$$\begin{cases} u = u_\infty \\ v = v_\infty \end{cases}, \begin{cases} \rho = \rho_\infty \\ P = P_\infty \end{cases}$$

and, at the outflow boundary (downstream), these quantities are extrapolated from the interior:

$$\frac{\partial u}{\partial n} = \frac{\partial v}{\partial n} = \frac{\partial \rho}{\partial n} = \frac{\partial P}{\partial n} = 0 .$$

2.4 Baldwin-Lomax turbulence model

The Baldwin and Lomax [37] turbulence model is an algebraic model for the determination of the eddy viscosity. μ_{turb} as a function of the local boundary layer velocity profile. The model is suitable for high-speed flows with thin attached boundary-layers, typically present in aerospace and turbomachinery applications. It is commonly used in quick design iterations where robustness is more important than capturing all details of the flow physics. The dual layered eddy viscosity formulation is sufficient to complete the Reynolds averaged Navier-Stokes (RANS) equation.

The Baldwin-Lomax approach separates the turbulence inside the boundary layer into two distinct regions: the inner

region and the outer region. Inside the inner region, typically very close to the wall

The turbulent eddy viscosity coefficient can be calculated as:

$$\frac{\mu_{turb}}{\mu_\infty} = \begin{cases} \mu_{turb_{inner}}, & \text{where } y < y_{crossover} \\ \mu_{turb_{outer}}, & \text{where } y > y_{crossover} \end{cases} \quad (14)$$

where $y_{crossover}$ is the smallest value of the dimensionless normal distance to the wall, $y_{crossover}$, at which the inner and outer eddy viscosity formulations produce the same result. Finally, after μ_{turb} calculation (for more details on this turbulence mode, the reader is advised to consult Baldwin and Lomax [37]), viscosity of flow will be defined as:

$$\mu = \mu_{lam} + \mu_{turb}, \quad (15)$$

where μ_{lam} is laminar flow viscosity that is defined by Sutherland equation defined as:

$$\mu_{lam} = \frac{(1.458\times10^{-6})T^{\frac{3}{2}}}{T+110.4}. \quad (16)$$

3. Numerical results and discussion

This section presents the results of simulations using both the Euler and the RANS equations with the Baldwin-Lomax turbulence model. Also, the numerical results are compared with experimental results. The parameters of each numerical simulation match the description of the experiments provided in Sec. 3.1.

3.1 Test cases

The pitching airfoils have an ample range of applications for validating numerical algorithms and their results are compared with experimental and other established numerical results. This research uses two different test cases, NACA 0012 airfoils (CT1 and CT5) and 64A010 airfoil (CT6). The important parameters used in the description of these cases are summarized in Table 1.

The sinusoidal pitching motion of the airfoils is given in terms of the variation of angle of attack as a function of time,

$$\alpha(t) = \alpha_m + \alpha_0 \sin(\omega t), \quad (17)$$

where α_m is the mean angle of attack, α_0 is the maximum pitching amplitude with respect to the mean and ω the angular velocity. In here, ω is expressed in terms of a non-dimensional parameter, which is called the reduced frequency (k_c). The reduced frequency is defined as:

$$k_c = \frac{\omega l_c}{2U_\infty}. \quad (18)$$

Table 1. Characteristics of the pitching airfoil test cases.

Description	Variable	Davis experiment	Landon experiment	Landon experiment
AGARD case number		CT6	CT5	CT1
Airfoil		NACA 64A010	NACA 0012	NACA 0012
Mean angle of attack	α_m	0.0°	0.016°	2.89°
Angle of attack variation	α_0	±1.01°	±2.51°	±2.41°
Reynolds number	Re_∞	12.56×10^6	5.5×10^6	4.8×10^6
Mach number	M_∞	0.796	0.755	0.6
Reduced frequency	k_c	0.202	0.0814	0.0808
Frequency (Hz):(1/Period)	f	50.32	62.5	34.4
Pitching axis (%chord root)	x_m	24.8	25	27.3

Here l_c, the characteristic length is the root chord length.

3.2 Computational grid

The first step in numerical discretization is to represent the continuous domain by a grid, where dependent variables of the governing equations are represented. Mesh generation has become an important field of study to enable solutions for more complex geometries. The choice of the type of mesh is usually based on the complexity of the geometry and the desired level of accuracy and approximation of the continuous problem.

In NACA 64A010 results section, where only the Euler equations are employed, large gradients close to the surface of the airfoil except for the shock wave do not exist and more uniform and regular meshes are sufficient to provide accurate numerical approximations (Figs. 2(a)-(c)). However, in NACA 0012 results section where the Navier-Stokes equations are used in the numerical simulation in a two-dimensional viscous flow environment, a high mesh resolution close to the surface of the airfoil is required to resolve the boundary layer and its interaction with the shock wave (Fig. 2(d)).

3.3 Mesh study

One of the important parts to confirm results of a numerical method is searching about independence of that method from a computational grid. In this context, mesh study has been done on the TSM results for one of the airfoils. Figs. 3 and 4

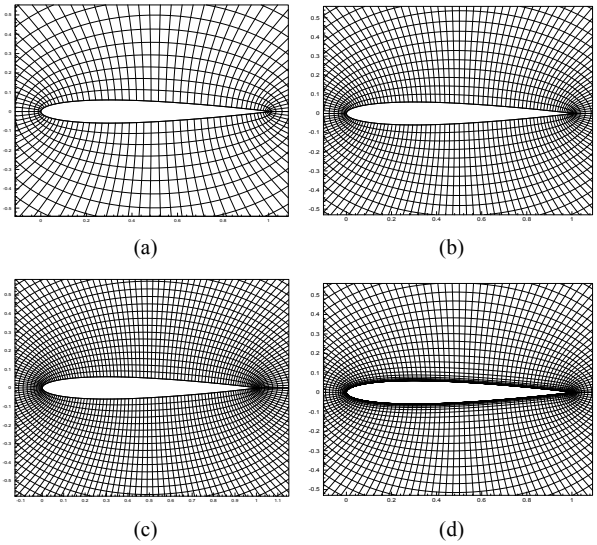

Fig. 2. Near field resolution of O-mesh grids: (a) 99x29 points used in the Euler calculations; (b) 149x51 points used in the Euler calculations for; (c) 179x81 points used in the Euler calculations for NACA 0012; (d) 149x51 points used in the unsteady Navier-Stokes calculations.

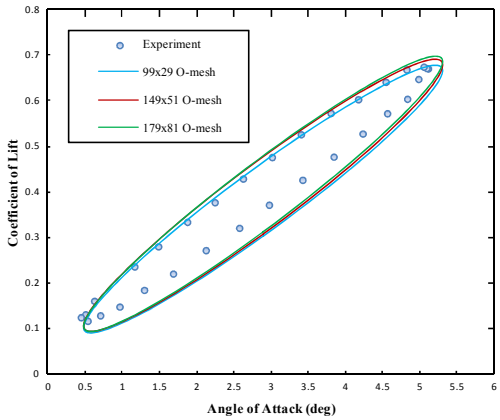

Fig. 3. Coefficient of lift as a function of angle of attack for various spatial resolutions-NACA 0012 (CT1).

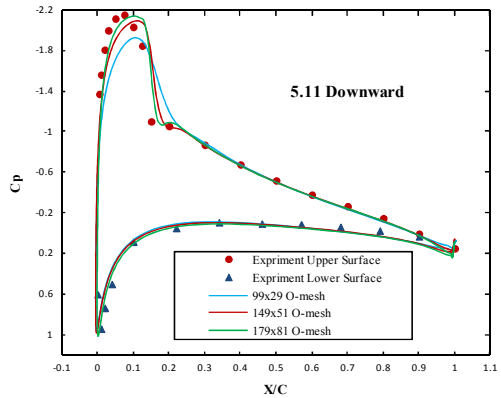

Fig. 4. Coefficient of pressure as a function of chord-wise distance for various spatial resolutions (CT1).

show results of coefficient of pressure (Cp) and coefficient of lift (Cl) for NACA 0012 (CT1) airfoil with different computational grid. The lift coefficient results do not show more changes for different grids (coarse, medium, fine and very fine grids). Therefore, it is better to analyze the results of the pressure coefficient in an angle in which shock waves occur.

It can be seen in the Fig. 4 that the mesh of 99*29 dimensions is not able to capture the shock wave produced in flow properly, but results for other grids are considerably alike and acceptable. The results presented in these figures show very little variation in the lift and pressure coefficients over the range of spatial resolutions. So the 179 * 81 grid point is used for the subsequent results to obtain accurate outcomes and save the computational time.

3.4 Inviscid results for NACA 64A010 airfoil

Coefficient of pressure results

Figs. 5 and 6 show both the numerical (TSM) and experimental Cp results along the NACA 64A010 airfoil at any quarter of a period (phase 0.0°, 90.0°, 180.0° and 270.0°) and NACA 0012 airfoil at an angle of attack that experimental data exist, respectively. Very good agreement between TSM and experimental results is evident. This shows the accuracy of TSM for the simulation of periodic transonic flows.

Since the Mach number of inflow in this NACA series is greater than that of NACA 0012, a sharper shock is created in the site of the shock wave, but with regard to smaller oscillation amplitude of this airfoil than that of model 0012, the magnitude of this shock is less, too. It has been seen that TSM can be applied accurately for ample range of variations of frequency and variations in angle of attacks.

Fig. 7 shows both the numerical and experimental Cl results as a function of the instantaneous angle of attack. A subfigure shows several ellipses each computed using a different number of time intervals. These plots show that the variation in time varying Cl as a function of the temporal resolution is negligible, and that results convergent to plotting accuracy can be obtained using only four time intervals.

3.5 Inviscid and viscous results for NACA 0012 airfoil

Coefficient of pressure results

Figs. 8(a) and (b) show both the numerical and experimental Cp results along the NACA 0012 airfoil for inviscid and viscous flow at an angle of attack that experimental data were exist. With comparison of Figs. 8(a) and (b) has been observed abrupt variation in Cp graphs that is produced due to shock wave, in viscous flow is smoother than inviscid flow because of boundary layer interaction with the shock wave.

Coefficient of lift results

Figs. 9(a) and (b) show both the numerical and experimental Cl results as a function of the instantaneous angle of attack for inviscid and viscous flow. In viscous results analysis has been used the Baldwin-Lomax turbulence model.

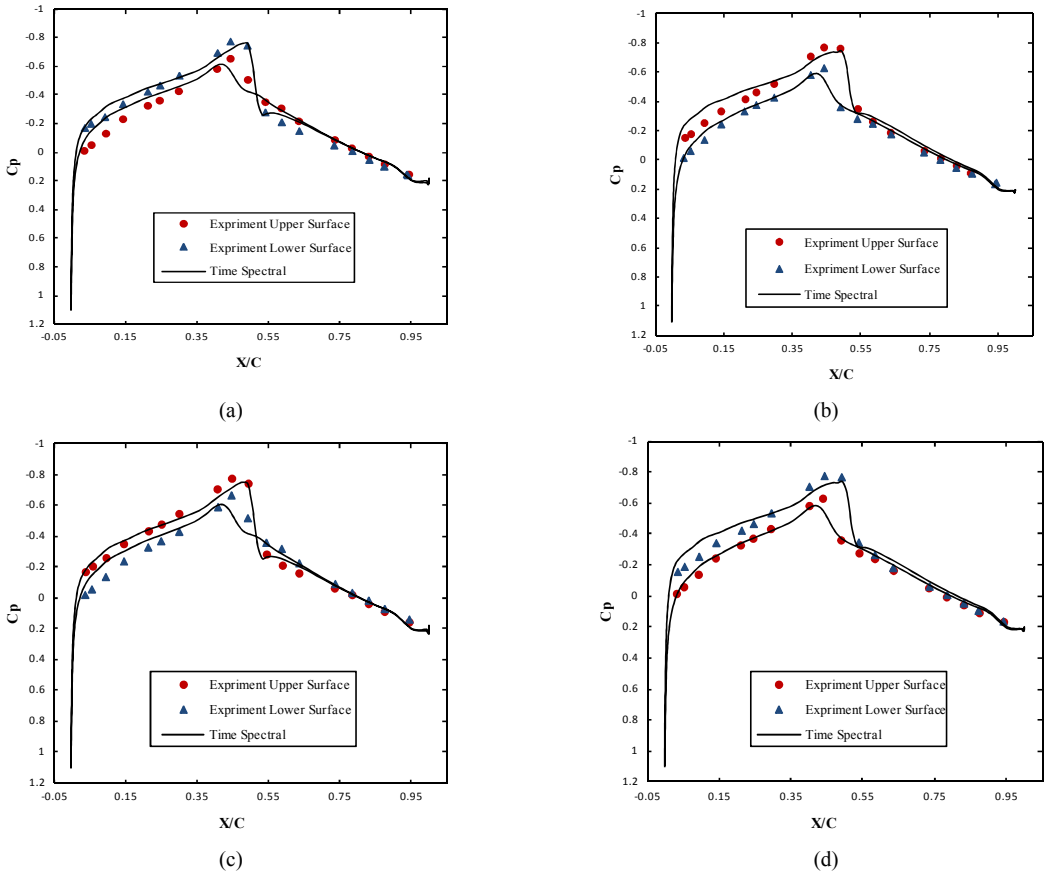

Fig. 5. Comparison of *Cp* numerical results with Davis's 64A010 experimental data: (a) $\alpha = 0.0°$ Upward, phase 0.0° ; (b) $\alpha = 1.01°$, phase 90.0° ; (c) $\alpha = 0.0°$ Downward, phase 180.0° ; (d) $\alpha = -1.01°$, phase 270.0° .

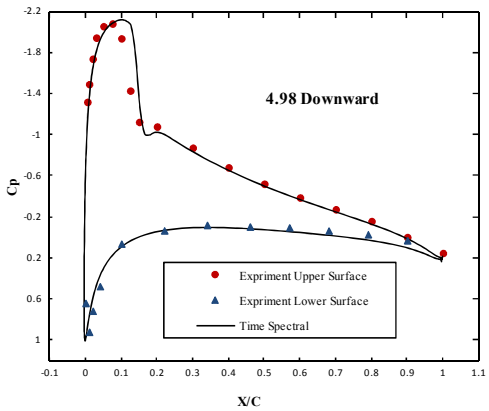

Fig. 6. Comparison of Cp numerical results with Landon's 0012 experimental data.

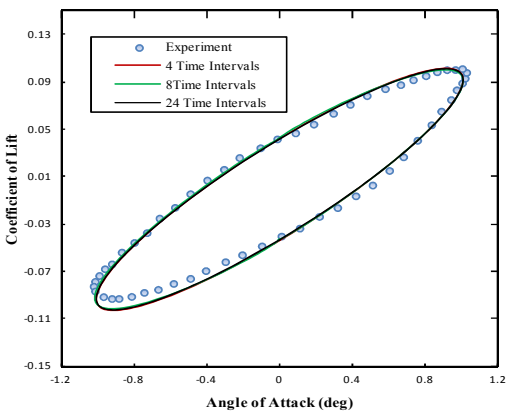

Fig. 7. Comparison Cl data as a function of the instantaneous angle of attack with Davis's 64A010 experiment results.

Instantaneous pressure distribution

Finally, Figs. 10(a) and (b) show instantaneous pressure distribution around pitching airfoil at maximum of pitch angle.

So that has been alluded to previously, because of boundary layer interaction with the shock wave in viscous flow, the shock wave is weaker than inviscid flow. It has been delineated by comparing Figs. 10(a) and (b).

3.6 A comparative analysis of TSM results with traditional methods

Three methods of solving the periodic aerodynamics problems are compared in Fig. 11. This figure shows Cl results of TSM, BDF and explicit structured adaptive grid methods for CT1 test case. All the computations were run on a Core™2

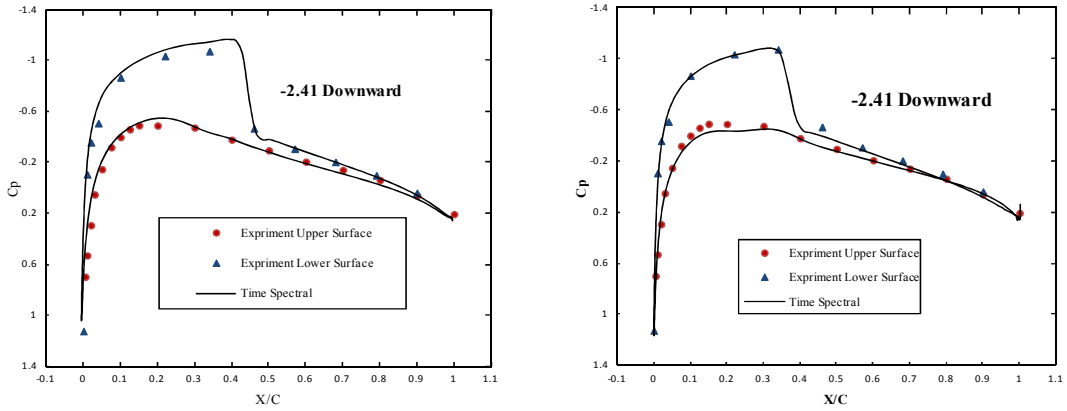

(a) (b)

Fig. 8. Comparison of Cp data with experimental results for NACA 0012 airfoil: (a) inviscid flow; (b) viscous flow.

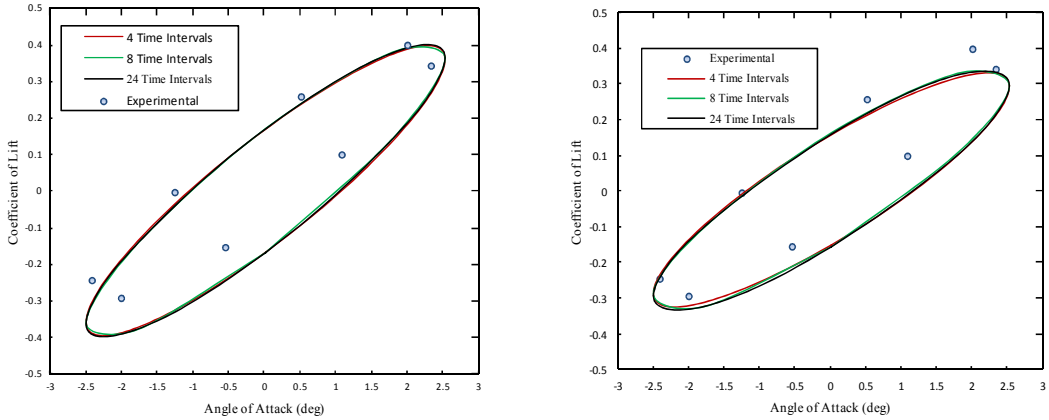

(a) (b)

Fig. 9. Comparison Cl data as a function of the instantaneous angle of attack with experimental results for the AGARD CASE: (a) inviscid flow; (b) viscous flow.

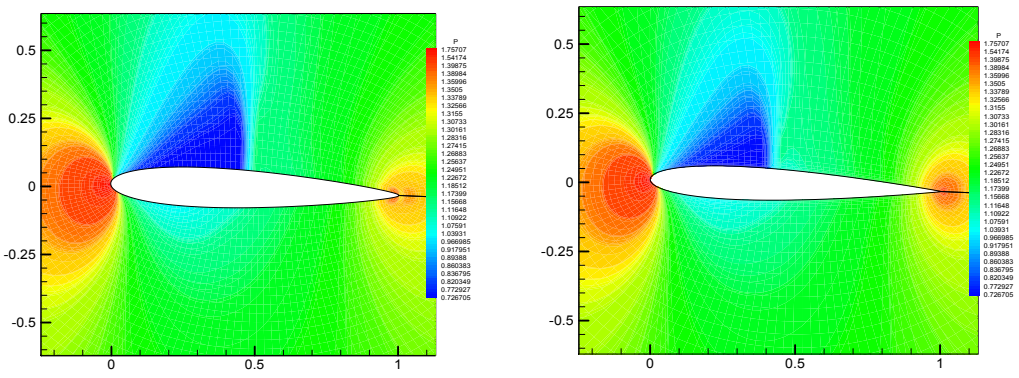

(a) (b)

Fig. 10. Instantaneous pressure distribution around CT5: (a) $\alpha = 2.526°$, inviscid flow; (b) $\alpha = 2.526°$, viscous flow equally spaced time levels.

Duo CPU, 2.66 MHz's. Explicit structured adaptive grid method requires 150 minutes for suitable convergence. But this time is only 8 minutes for the TSM on the same processor and the same grid. Also, 200 time intervals are required using BDF method for convergence, while the TSM offers these results somewhat better in respect to accuracy and with only four time intervals, although the memory requirement for TSM is greater than other two methods. These differences are

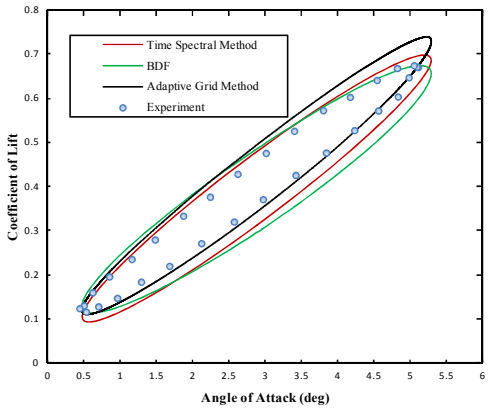

Fig. 11. Comparison of the time spectral method Cl data results with BDF and explicit structured adaptive grid method results (CT1).

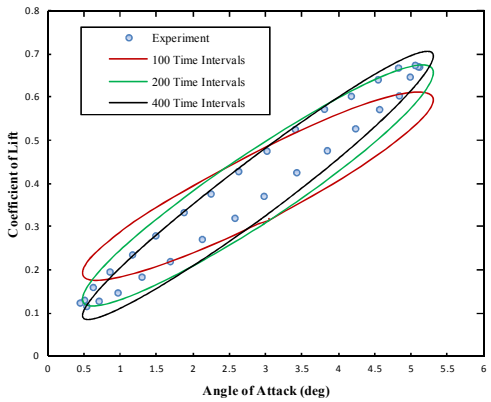

Fig. 12. Coefficient of Lift numerical result using BDF per different time intervals for NACA 0012 (CT1).

significant, especially for three-dimensional problems. This means that the TSM is a fast and efficient method for the unsteady periodic problems. It is noteworthy that these comparisons are meaningful and acceptable since spatial discretization methods are identical among all the techniques and the only difference is in calculating temporal derivative and solution algorithm in various time steps in a period.

Fig. 12 shows *Cl* results using BDF for different time intervals. It should be noted that unlike TSM, increasing the number of intervals (reducing time steps) increases the accuracy of the outcomes. This means that the solution time increases.

Comparing the results of Figs. 11 and 12 presents the advantage of TSM in numerical simulations of periodic unsteady problems with the number of small time intervals, resulting in greater convergence rate while maintaining the desired accuracy. This advantage of TSM in analysis of three-dimensional problems is more specific, where due to prolonged calculation, it is very time consuming to choose too small time steps to reach to a convergent solution, and it is essential to accelerating solution time by fewer number of time steps (larger time steps).

4. Conclusions

The time spectral method is an intense method in time-periodic unsteady flow analysis. So that presents a proper accuracy of the solution and a low time for convergence. Conforming to a time accurate existing solver is another preference of this method. TSM performs all the calculations in the time domain, and hence requires minimal modifications to an existing solver.

TSM algorithm is simpler to implement than the typical NLFD solver because it does not require the multiple operations of Fourier transforms and inverse Fourier transforms, while still achieving better convergence and reducing computational cost in comparison to the typical traditional schemes such as BDF and explicit structured adaptive grid. This work shows that time intervals are sufficient to successfully capture the unsteady periodic flow by TSM. This is much less than the number of time intervals required for traditional schemes.

The TSM algorithm is able to numerically simulate and capture the flow physics around pitching airfoils at both cases including strong shock waves (NACA 64A010 (CT6) and weak shock waves (NACA 0012 (CT1 and CT5).

The Baldwin-Lomax model is suitable for high-speed flows with thin attached boundary-layers, typically present in aerospace and turbomachinery applications. The model is not suitable for cases with large separated regions and significant curvature/ rotation effects. But it is a reliable model very simple to implement and popular for CFD applications.

References

[1] W. J. McCroskey, Inviscid flow field of an unsteady airfoil, *AIAA Journal*, 11 (1973) 1130-1137.

[2] W. J. McCroskey, Unsteady airfoils, *Annual Review of Fluid Mechanics*, Palo Alto, CA, 14 (1982) 285-311.

[3] R. D. Rausch, Z. Yang, T. Y. Henry and J. T. Batina, Euler flutter analysis of airfoils using unstructured dynamic meshes, *Journal of Aircraft*, 27 (5) (1990) 436-443.

[4] J. M. Anderson, K. Streitlien, D. S. Barrett and M. S. Triantafyllou, Oscillating foils of high propulsive efficiency, *Journal of Fluid Mechanics*, 360 (1998) 41-72.

[5] S. Mittal, Finite element computation of unsteady viscous compressible flows, *Computer Methods in Applied Mechanics and Engineering*, 157 (1-2) (1998) 151-175.

[6] Z. Yang, L. N. Sankar, M. Smith and O. Bauchau, Recent improvements to a hybrid method for rotors in forward flight, Presented as Paper 2000-0260 at the AIAA 38th Aerospace Sciences Meeting & Exhibit, Reno, NV, (January 2000), *Journal of Aircraft*, 39 (5) (2002) 804-812.

[7] Q. J. Zhao, G. H. Xu and G. J. Zhao, New hybrid method for predicting the flowfields of helicopter rotors, *Journal of Aircraft*, 43 (2) (2006) 372-380.

[8] S. Yang, Z. Zhang, F. Liu, S. Luo, H. M. Tsai and D. Schuster, Time-domain aeroelastic simulation by a coupled euler and integral boundary-layer method, *22nd Applied Aerody-*

namics Conference and Exhibit, Rhode, Island (2004).

[9] J. M Hsu and A. Jameson, An implicit-explicit hybrid scheme for calculating complex unsteady flows, *40th AIAA Aerospace Sciences Meeting and Exhibit*, Reno, Nevada (2002).

[10] S. K. Nadarajah and A. Jameson, Optimal control of unsteady flows using a tim accurate method, *9th AIAA/ISSMO Symposium on Multidisciplinary Analysis and Optimization Conference*, Atlanta, GA (2002).

[11] J. M. J. Hsu, *An implicit-explicit flow solver for complex unsteady flows*, Stanford University (2004) 206.

[12] Z. Zhang, F. Liu and D. M. Schuster, Calculations of unsteady flow and flutter by an euler and integral boundary-layer method on cartesian grids, *22nd Applied Aerodynamics Conference and Exhibit*, Rhode Island (2004).

[13] M. Pasandideh Fard, A. Heidary and M. Malek-jafarian, Numerical Analysis of Unsteady Flow around a Oscillator Airfoil with Moving Structured Adaptive Grid by Using Central and Upwind Schemes, *International Aerospace Conference*, Ankara, August 17-19 (2009).

[14] K. C. Hall, J. P. Thomas and W. S. Clark, Computation of Unsteady Nonlinear Flows in Cascades Using a Harmonic Balance Technique, 9th International Symposium on Unsteady Aerodynamics, Aeroacoustics and Aeroelasticity of Turbomachines (ISUAAAT), Lyon, France, (2000), *AIAA Journal*, 40 (5) (2002) 879-886.

[15] J. P. Thomas, K. C. Hall and E. H. Dowell, A harmonic balance approach for modeling nonlinear aeroelastic behavior of wings in transonic viscous flow, *AIAA/ASME/ASCE/AHS/ASC Structures, Structural Dynamics and Materials Conference*, 7 (2003) 4779 - 4784.

[16] J. P. Thomas, E. H. Dowell, K. C. Hall and C. M. Denegri, Further investigation of modeling limit cycle oscillation behavior of the F-16 fighter using a harmonic balance approach, *Collection of Technical Papers - AIAA/ASME/ASCE/AHS/ASC Structures, Structural Dynamics and Materials Conference*, 3 (2005) 1457-1466.

[17] J. P. Thomas, C. H. Custer, E. H. Dowell and K. C. Hall, Unsteady flow computation using a harmonic balance approach implemented about the overflow 2 flow solver, *AIAA Paper 2009-4270*, *19th AIAA Computational Fluid Dynamics Conference*, San Antonio, TX, June (2009).

[18] M. A. Spiker, J. P. Thomas, R. E. Kielb, K. C. Hall and E. H. Dowell, Modeling cylinder flow vortex shedding with enforced motion using a harmonic balance approach, *AIAA Paper 2006-1965, 47th AIAA/ASME/ASCE/AHS/ASC Structures, Structural Dynamics and Materials (SDM) Conference*, Newport, RI, May (2006).

[19] L. Liu, J. P. Thomas, E. H. Dowell, P. J. Attar and K. C. Hall, A comparison of classical and high dimensional harmonic balance approaches for a duffing oscillator, *Journal of Computational Physics*, 215 (1) (2006) 298-320.

[20] L. Liu, E. H. Dowell and J. P. Thomas, A high dimensional harmonic balance approach for an aeroelastic airfoil with cubic restoring forces, *Journal of Fluids and Structures*, 23 (3) (2007) 351-363.

[21] A. Da Ronch, M. Ghoreyshi , K. J. Badcock, S. Goertz, M. Widhalm, R. P. Dwight and M. S. Campobasso, Linear frequency domain and harmonic balance predictions of dynamic deritvates, *28th AIAA Applied Aerodynamics Conference*, Chicago, USA, 28 Jun-1 Jul (2010).

[22] M. McMullen, A. Jameson and J. J. Alonso, Application of a nonlinear frequency domain solver to the Euler and Navier-Stokes equations, *AIAA paper 02-0120, AIAA 40th Aerospace Sciences Meeting and Exhibit,* Reno, NV, January (2002).

[23] M. McMullen and A. Jameson, The computational efficiency of non-linear frequency domain methods, *Journal of Computational Physics*, 212 (2006) 637-661.

[24] M. McMullen, A. Jameson and J. J. Alonso, Demonstration of nonlinear frequency domain methods, *AIAA Journal*, 44 (7) (2006) 1428-1435.

[25] S. K. Nadarajah, A. Jameson and M. McMullen, Non-linear frequency domain based optimum shape design for unsteady three-dimensional flow, *44th AIAA Aerospace Sciences Meeting and Exhibit*, Reno, NV, January 9-12 (2006).

[26] K. Nadarajah and A. Jameson, Optimum shape design for unsteady three-dimensional viscous flows using a NLFD method, *AIAA Journal of Aircraft*, 44 (5) (2007) 1513-1527.

[27] J. S. Cagnone and S. Nadarajah, An implicit non-linear frequency domain-spectral difference scheme for periodic Euler flow, *AIAA Journal*, 47 (2) (2009) 361-372.

[28] A. Mosahebi and S. Nadarajah, Dynamic mesh deformation for implicit adaptive non-linear frequency domain method, *Seventh International Conference on Computational Fluid Dynamics (ICCFD7)*, Big Island, Hawaii, July 9-13 (2012).

[29] A. K. Gopinath and A. Jameson, Time spectral method for periodic unsteady computations over two- and three- dimensional bodies, *AIAA Paper 2005-1220, AIAA 43th Aerospace Sciences Meeting & Exhibit*, Reno, NV, 10683-10696 (2005).

[30] N. Butsuntorn and A. Jameson, Time spectral method for rotorcraft flow, *46th AIAA Aerospace Sciences Meeting and Exhibit,* Reno, NV, *AIAA Paper 2008-0403* (2008).

[31] N. Butsuntorn and A. Jameson, Time spectral method for rotorcraft flow with vorticity confinement, *26th AIAA Applied Aerodynamics Conference*, Honolulu, HI, August 18-21 (2008).

[32] F. Sicot, G. Puigt and M. Montagnac, Block-Jacobi implicit algorithms for the time spectral method, *AIAA Journal,* 46 (12) (2008) 3080-3089.

[33] X. Su and X. Yuan, Implicit solution of time spectral method for periodic unsteady flows, *International Journal for Numerical Methods in Fluids,* 860-876 (2009).

[34] Z. Yang and D. Mavriplis, Time spectral method for periodic and quasi-periodic unsteady computations on unstructured meshes, *40th AIAA Fluid Dynamics Conference*, Illinois, June 28-1 (2010).

[35] Z. Yang, D. Mavriplis and J. Sitaraman, Prediction of helicopter maneuver loads using BDF/time spectral method on unstructured meshes, *49th AIAA Aerospace Sciences Meeting*, Florida, Jan. 4-7 (2011).

[36] S. Antheaume and C. Corre, Implicit time spectral method

for periodic incompressible flows, *AIAA Journal*, 49 (4) (2011) 791-805.
[37] B. S. Baldwin and H. Lomax, Thin layer approximation and algebraic model for separated turbulent flows, *AIAA Paper 78 257* (1978).
[38] L. Prandtl, Bericht uber untersuchugen zur ausgebildeten turbulenz, *Z. Angew Math*., *Meth*., 5 (1925) 136-139.
[39] T. Cebeci and A. M. O. Smith, *Analysis of turbulent boundary layers,* Academic Press, New York (1974).
[40] S. S. Davis, NACA 64A010 (NASA Ames Model) Oscillatory Pitching, *AGARD Report 702, AGARD, Dataset 2*, January (1982).
[41] R. H. Landon, NACA 0012 Oscillatory and transient pitching, *AGARD Report 702, AGARD, Dataset 3,* January (1982).
[42] A. Jameson, W. Schmidt and, E. Turkel, Numerical solutions of the Euler equations by finite volume methods with Runge-Kutta time stepping schemes, *AIAA paper 81-1259,* January (1981).
[43] P. Moin, *Spectral methods in computational physics*, Supplementary notes*,* Stanford University, Stanford, CA, ME 408 (2003).
[44] A. Jameson, *Numerical methods in fluid dynamics*, Lecture Notes in Mathematics, 1127 (1985), chap. Transonic Flow Calculations, 156-242. Springer Berlin/Heidelberg, Princeton University MAE Report 1651, March (1984).

Mohamad Reza Mohaghegh received the B.S. degree in Fluid Mechanics from the University of Kerman (Iran) on 2007, M.S. degree in Energy Conver- sion from Uni- versity of Birjand (Iran) in 2010. His research interests include computational fluid dynamics, aerodynamics, heat transfer, analytical methods in engineering. He is a research associate in the Mechanical Engineering Department of Ferdowsi University of Mashhad and a member of Young Researchers and Elite Club at Islamic Azad University (Iran).

Majid Malek-Jafarian received B.S. degree in Fluid Mechanics from Ferdowsi University of Mashhad(Iran) on1997, M.S. degree in Energy Conversion from Ferdowsi University in 1999 and Ph.D. in Energy Conversion from Mechanical Engineering department of Ferdowsi University of Mashhad(Iran) on 2006. His major field of study is turbulence modeling, aerodynamics and optimization. Now he's working at the Mechanical Engineering Department of the University of Birjand.